Minimal models for Wannier-type higher-order topological insulators and phosphorene

Motohiko Ezawa

Phys. Rev. B **98**, 045125 — Published 18 July 2018

DOI: 10.1103/PhysRevB.98.045125

Minimal models for Wannier-type higher-order topological insulators and phosphorene

Motohiko Ezawa
Department of Applied Physics, University of Tokyo, Hongo 7-3-1, 113-8656, Japan

A higher order topological insulator (HOTI) is an extended notion of the conventional topological insulator. It belongs to a special class of topological insulators to which the conventional bulk-boundary correspondence is not applicable. Provided the mirror symmetries are present, the bulk topological number is described by the quantized Wannier center located at a high symmetry point of the crystal. The emergence of corner states is a manifestation of nontrivial topology in the bulk. In this paper we propose minimal models for the Wannier-type second-order topological insulator in two dimensions and the third-order topological insulator in three dimensions. They are anisotropic chiral-symmetric two-band models. It is explicitly shown that the Wannier center is identical to the winding number in the present model, demonstrating that it is indeed a topological quantum number. Finally we point out that the essential physics of phosphorene near the Fermi energy is described by making a perturbation of the Wannier-type HOTI. We predict that these corner states will be observed in the rhombus structure of phosphorene near the Fermi energy around -0.16eV.

A topological insulator (TI) is characterized by the bulk topological number together with the emergence of topological boundary states[1,2]. The gap must close along the boundary since the topological number cannot change its value continuously across the boundary, which is known as the bulk-boundary correspondence. The typical bulk topological number is the Chern number, which is the genuine one. Another typical one is the Z_2 index, which is protected by the time-reversal symmetry. Recently, the concept of the TI has been generalized to include the higher-order TI (HOTI)[3–12]. Let us consider a j-dimensional (jD) bulk system. For instance, a second-order TI is an insulator which has $(j-2)$D topological boundary states but no $(j-1)$D topological boundary states. Similarly, a third-order TI is an insulator which has $(j-3)$D topological boundary states but no $(j-1)$D and $(j-2)$D topological boundary states. Namely, the boundary of the third-order TI is the second-order TI. In spite of these properties, the HOTI is also characterized by the bulk topological number[4,8,9,12]. It belongs to a special class of TIs where the bulk-boundary correspondence is appropriately generalized. Accordingly, a new possibility has arisen that an insulator previously considered trivial can be a HOTI.

Recent studies have revealed a crucial role that the Wannier center (WC) plays in a certain type of HOTIs[4,8,9,12]. The WC is defined by the expectation value of the position in the unit cell of a crystal. It had been considered[13,14] that the system is trivial when Wannier functions are constructed for all filled bands. However, it was pointed out[8] that the system can be somewhat nontrivial if there is a mismatch between the WC and the lattice sites. In this paper, by taking instances of mirror symmetric models, we show that the WC is quantized and fixed at a high-symmetry point with respect to the mirror symmetries. It can be used as a new type of the topological quantum number[4,9,12] because it is quantized and cannot change its value without gap closing. We conclude that the system is second-order topological when the Wannier center is away from the lattice sites.

We propose the minimal models of Wannier-type HOTIs in two and three dimensions. They are given by chiral-symmetric two-band models. We demonstrate the topological nature of the WC explicitly by showing that it is equivalent to a set of the winding numbers. We first analyze a 2D crystal (anisotropic honeycomb lattice) as the minimal model. We calculate the energy spectra for the bulk, a nanoribbon[15] and a nanodisk[16] to search for boundary states. Topological boundary states emerge as corner states when the WC is nontrivial. It is also possible to construct a 3D crystal (anisotropic diamond lattice) so that its boundary is the above 2D crystal (anisotropic honeycomb lattice) when we cut it along a plane. Then, it is a third-order TI by definition. These anisotropic lattice models are higher-dimensional extensions of the Su-Schrieffer-Heeger (SSH) model[17].

We then investigate the physics of phosphorene in the vicinity of the Fermi energy, where it is well described by a two-band model. Although it is not chiral symmetric, we can analyze it by making a perturbation of a Wannier-type HOTI. In particular, a rhombus structure has two topological corner states near the Fermi energy around -0.16eV.

Minimal two-band models: HOTIs were originally proposed on square lattices with the use of the four-band model[3–11], and subsequently studied on the breathing Kagome and pyrochlore lattices with the use of the three-band and four-band models[12], respectively. The minimal model to describe insulators is obviously the two-band model. We propose a two-band model to reveal the essence of HOTIs.

We consider lattice models which have two atoms in the unit cell. We take the two-band Hamiltonian,

$$H = \begin{pmatrix} f & F \\ F^* & f \end{pmatrix} \equiv H_0 + fI, \tag{1}$$

where I is the 2×2 identity matrix. The Hamiltonian H has the mirror symmetry,

$$M_\alpha^{-1} H(k_\alpha) M_\alpha = H(-k_\alpha), \tag{2}$$

with $M_\alpha = i\sigma_\alpha$. The term H_0 is chiral symmetric,

$$C^{-1} H_0(k_\alpha) C = -H_0(k_\alpha) \tag{3}$$

with $C = \sigma_z$. The diagonal element f breaks the chiral symmetry.

The energy spectrum reads $E = f \pm |F|$. As typical examples of F, we take the following functions: (i) In the case of one dimension, we consider the SSH chain with[17]

$$F = t_a + t_b e^{ik}. \tag{4}$$

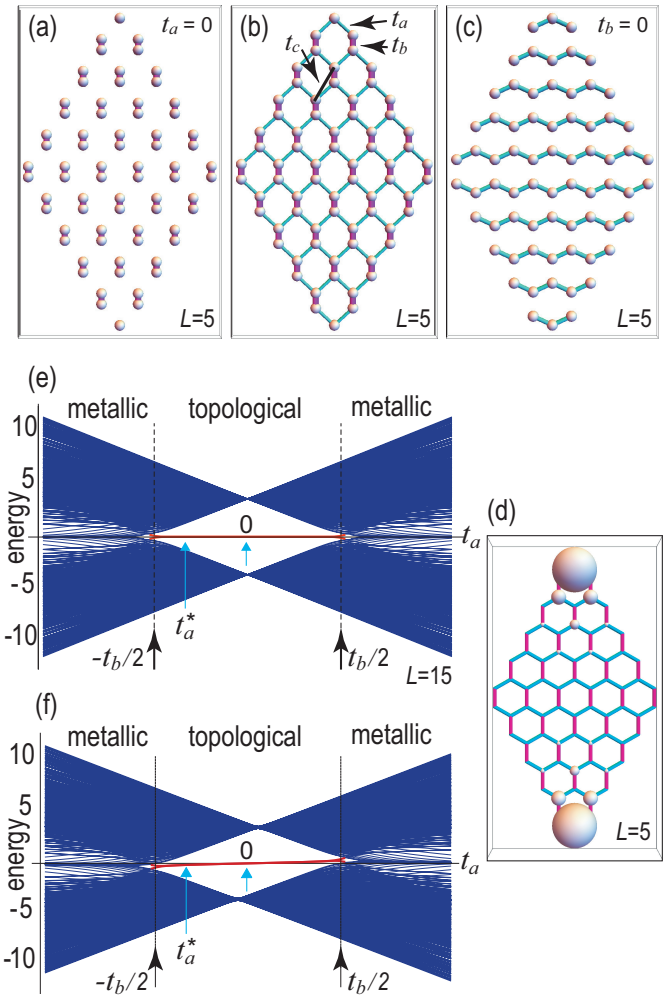

FIG. 1: Illustration of rhombuses with (a) $t_a = 0$, (b) $|t_a| < t_b$ and (c) $t_b = 0$. The size L is defined by the number of Benzene rings on one side in (b). Here, $L = 5$. There are two isolated atoms at the top and bottom corners of the rhombus for $t_a = 0$ in (a). (d) The square root of the local density of states $\sqrt{\rho_i}$ for the rhombus. The amplitude is represented by the radius of the spheres. (e) Energy spectrum of the rhombus made of the anisotropic honeycomb lattice. There emerge topological corner states (marked in red) at the Fermi energy for $|t_a| < t_b/2$. (f) Energy spectrum of the rhombus made of phosphorene. The horizontal axis is t_a. We have chosen the parameters as $t_b = 3.665$eV, $t_c = -0.105$eV and $t_a^* = -1.220$eV for phosphorene.

(ii) In the case of two dimensions, we consider the anisotropic honeycomb lattice with[18–22]

$$F = 2t_a e^{-ik_y/2} \cos\frac{\sqrt{3}k_x}{2} + t_b e^{ik_y}. \tag{5}$$

(iii) In the case of three dimensions, we consider the anisotropic diamond lattice with[23]

$$F = t_a \left(e^{i\mathbf{k}\cdot\mathbf{X}_2} + e^{i\mathbf{k}\cdot\mathbf{X}_3} + e^{i\mathbf{k}\cdot\mathbf{X}_4}\right) + t_b e^{i\mathbf{k}\cdot\mathbf{X}_1}, \tag{6}$$

with the four lattice vectors pointing the tetrahedron directions $\mathbf{X}_1 = (1,1,1)$, $\mathbf{X}_2 = (1,-1,-1)$, $\mathbf{X}_3 = (-1,1,-1)$ and

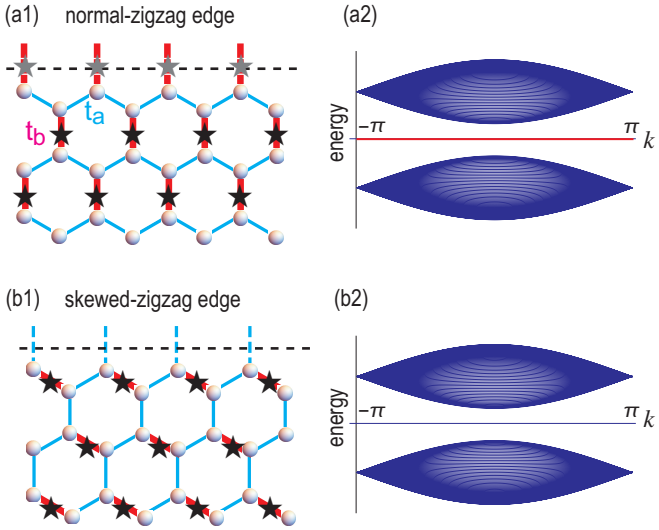

FIG. 2: Illustration and band structure of (a1,a2) a normal-zigzag nanoribbon and (b1,b2) a skew-zigzag nanoribbon, where $t_a = -1.220$eV, $t_b = 3.665$eV and $t_c = -0.105$eV. Star symbols represent WCs in (a1,b1). The horizontal axis is k in (a2,b2). (a2) When the edge cuts through WCs as in (a1), perfect flat bands emerge at the Fermi energy (red line). These perfect flat bands do not represent topological edge states. (b2) When the edge cuts through no WCs as in (b1), no edge states emerge at the Fermi energy.

$\mathbf{X}_4 = (-1,-1,1)$. We take $t_b > 0$ without loss of generality. The function f is arbitrary. Later we take an example in two dimensions to describe phosphorene: See (10).

In the case of the SSH model ($f = 0$), the WC is given by the polarization P_x along the x axis, which is the bulk topological number protected by the mirror symmetry along the x direction. It has been generalized to higher dimensions[4,8,9,12].

Actually, the WC is well defined in the models even for $f \neq 0$. It is given by the set of the j polarization P_α in the j dimensions, which is the average of the position in the unit cell. The polarization P_α is formulated as

$$P_\alpha = -\frac{1}{V}\int_{\mathrm{BZ}} d^j k A_\alpha, \tag{7}$$

where $A_\alpha = -i\langle\psi|\partial_{k_\alpha}|\psi\rangle$ is the Berry connection, V is the volume of the Brillouin zone, and the integration is carried out over the Brillouin zone. It is easy to check that the Berry connection is independent of f. Now, due to the gauge invariance of the polarization[4], P_α is defined mod 1. Furthermore, due to the mirror symmetry (2), the polarization is odd[4], $P_\alpha \to -P_\alpha$, with respect to $k_\alpha \to -k_\alpha$. Combining these two properties, we find[4,8,9,12] that P_α is quantized to be 0 or $1/2$. As we shall show, the WC is located at $1/2$ for the SSH chain, $(0, 1/2)$ for the anisotropic honeycomb lattice and $(1/2, 1/2, 1/2)$ for the anisotropic diamond lattice. They are the centers of the dimerized bonds, representing the high-symmetry points with respect to the mirror symmetry.

The WC is quantized as long as the system remains to be an insulator since the integration is taken over the whole the Brillouin zone. The WC cannot change its value unless the

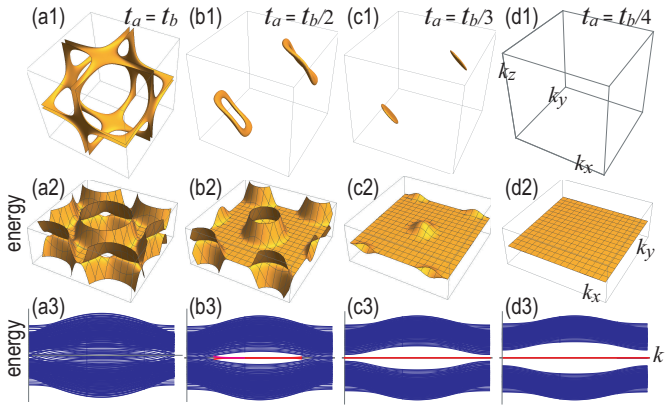

FIG. 3: The Fermi surface of the bulk anisotropic diamond lattice with (a1) $t_a = t_b$, (b1) $t_a = t_b/2$, (c1) $t_a = t_b/3$ and (d1) $t_a = t_b/4$. (a2)-(d2) The corresponding band structure of a thin film. (a3)-(d3) The corresponding band structure of a diamond prism. The size of the diamond is $L = 3$.

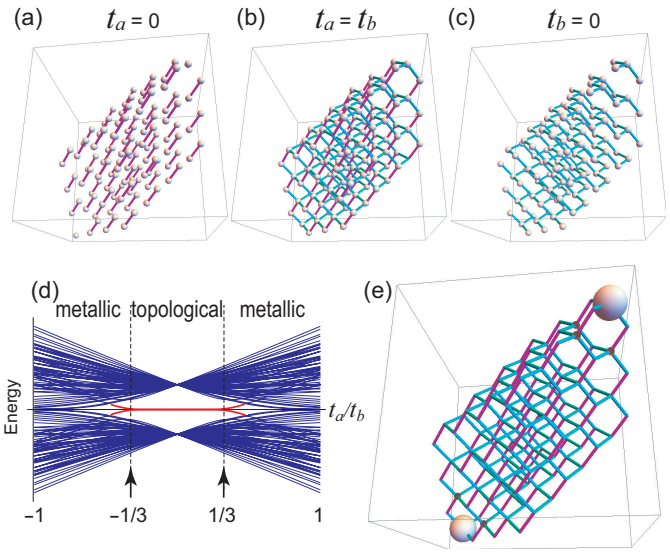

FIG. 4: Illustration of a rhombohedron made of the diamond lattice with (a) $t_a = 0$, (b) $t_a = t_b$ and (c) $t_b = 0$. (d) Energy spectrum of the rhombohedron made of the anisotropic diamond lattice with $L = 3$. The horizontal axis is t_a/t_b. There emerge zero-energy states (marked in red) for $|t_a/t_b| < 1/3$. They are topological boundary states. (e) The square root of the local density of states $\sqrt{\rho_i}$ for the rhombohedron with $L = 3$ and $t_a/t_b = 1/4$. The amplitude is represented by the radius of the spheres.

bulk band gap closes as a function of t_α/t_b. The WC may be used as the bulk topological number.

We are able to make manifest the topological nature of the polarization by relating it with the winding number. Using the Hamiltonian (1) explicitly, we may solve for the eigen function of the ground state as $\psi = \left(-e^{-i\Theta}, 1\right)^t/\sqrt{2}$ with $\Theta = i\log(F/|F|)$. The connection reads

$$A_\alpha = -\frac{1}{2}\partial_{k_\alpha}\Theta, \tag{8}$$

and hence the formula (7) represents the winding number.

Anisotropic honneycomb lattice as a HOTI: We now show that the chiral symmetric two-band model H_0 describes a second-order TI in the range of parameters $|t_a| < t_b/2$ by making four-step arguments. We calculate the energy spectra for the bulk, the nanoribbon and the nanodisk in the first three steps. Finally we make the topological arguments.

(i) First, we examine the bulk band spectrum. The dispersion relation reads

$$E = \pm\sqrt{t_b^2 + 4\left(t_a^2 + t_a t_b \cos\frac{\sqrt{3}}{2}k_x\right)\cos\frac{k_y}{2}}. \tag{9}$$

The system becomes an insulator for $|t_a| < t_b/2$.

ii) Second, we study the energy spectrum of the 1D boundary (edges) by calculating the band structure of a normal-zigzag nanoribbon[22], where the edge passes through the WCs, as in Fig.2(a1). There exist perfect flat bands near the Fermi energy for $|t_a| < t_b/2$, as depicted in red in Fig.2(a2). However, they are not topological edge states implied by the conventional bulk-edge correspondence, since they are entirely detached from the bulk band.

The emergence of these edge states is understood as follows. The WC exists at the middle of the bond connecting the A and B sites, as illustrated in Fig.2(a1). The charge distributes in the vicinity of the WCs. The charge is separated into two pieces by the boundary on the WCs, yielding a half charge at the boundary to form edge states as in Fig.2(a2).

On the other hand, there are no edge states in a skew-zigzag nanoribbon[25]: See Fig.2(b2). This is because the edges pass through no WCs when we cut a crystal along a line to create a edge, as illustrated in Fig.2(b1).

iii) Third, we study the energy spectrum of the 0D boundary (corners) by calculating the band structure of a nanodisk respecting the mirror symmetries. The simplest one is the rhombus structure with four skew-zigzag edges as in Fig.1(e). In contrast to the 1D boundary, zero-energy topological boundary states emerge at the corners of a nanodisk protected by both the mirror symmetries and the chiral symmetry. Corner states emerge at the top and bottom lattice sites for $|t_a| < t_b/2$ [Fig.1(d)]. When we put one electron into the corner states, the $1/2$ fractional charge appears at each of the two corners of the rhombus. They are absorbed in metallic phase for $|t_a| > t_b/2$.

(iv) Finally, we study the WC, which is the bulk topological number characterizing the HOTI. We first investigate the extreme case of $t_a = 0$. The eigen function for the valence band is given by $\psi = \left(-e^{ik_y}, 1\right)/\sqrt{2}$. The Berry connections are obtained as $A_x = 0$ and $A_y = 1/2$, which yields the WC as $(0, 1/2)$. Since the position of the WC is fixed within one topological phase, we obtain the same result for $|t_a| < t_b/2$. The gap closes at $|t_a| = t_b/2$, and the system becomes metallic for $|t_a| > t_b/2$ as shown in Fig.1(e).

Phosphorene: The anisotropic honeycomb lattice is realized in phosphorene[22], which is a monolayer material of black phosphorus. Phosphorene is well described in the vicinity of

the Fermi energy by the two-band Hamiltonian H given by (1) with (5) and

$$f = 4t_c \cos\frac{\sqrt{3}}{2}k_x \cos\frac{1}{2}k_y. \tag{10}$$

Three hopping parameters t_a, t_b and t_c are shown in Fig.1(b), which are $t_a = -1.220$eV, $t_b = 3.665$eV, $t_c = -0.105$eV according to Ref.[24]. The Hamiltonian H is not chiral symmetric due to the diagonal term f. Since $|f| \leq 4|t_c| = 0.42$eV, we may treat the term by way of a perturbation. We calculate numerically the band structure to find that the modification is negligible from its chiral-symmetric limit: See Fig.1(f). In particular, we predict that the corner states emerge around -0.16eV.

Anisotropic diamond lattice as a HOTI: We proceed to investigate the anisotropic diamond lattice in three dimensions. We make the five-step arguments based on the chiral symmetric model by setting $f = 0$ in the Hamiltonian (1) with (6).

i) The bulk band spectrum reads

$$\begin{aligned} E^2 =& t_a^2 + 3t_b^2 + 2t_b^2\cos 2\left(k_x - k_y\right) + 2t_b^2\cos 2\left(k_y - k_z\right) \\ &+ 2t_b^2\cos 2\left(k_z - k_x\right) + 2t_a t_b\cos 2\left(k_x + k_y\right) \\ &+ 2t_a t_b\cos 2\left(k_y + k_z\right) + 2t_a t_b\cos 2\left(k_z + k_x\right). \end{aligned} \tag{11}$$

We show the Fermi surface in Fig.3(a1)-(d1). The Fermi surface becomes a loop node for $t_b/3 < |t_a| < t_b$, whose radius shrinks as the ration $|t_a/t_b|$ decreases as in Fig.3(b1) and (c1). The system becomes an insulator for $|t_a| < t_b/3$ as in Fig.3(d1).

ii) We calculate the surface band structure of a thin film in the [111] direction corresponding to the $(j-1)$D geometry with $j = 3$. Zero-energy partial flat bands appear whose boundary is the projection of the loop node onto the [111] direction for $t_b/3 < |t_a| < t_b$: See Fig.3(b2) and (c2). It becomes a perfect flat band for $|t_a| < t_b/3$ corresponding to the fact that the the system becomes an insulator: See Fig.3(d2).

iii) We next calculate the band structure of a diamond prism corresponding to the $(j-2)$D geometry with $j = 3$. As in the case of the thin film, we find partial flat bands at zero-energy for $t_b/3 < |t_a| < t_b$ [Fig.3(b3), (c3)], and perfect flat bands at zero-energy for $|t_a| < t_b/3$ [Fig.3(d3)].

iv) We investigate the energy spectrum of the rhombohedron made of the diamond lattice, which corresponds to the $(j-3)$D geometry with $j = 3$: See Fig.4. The energy spectrum as a function of t_a/t_b is shown in Fig.4(d). The zero-energy states emerge for $|t_a| < t_b/3$. The emergence of the zero-energy states are naturally understood by considering the extreme case with $t_a = 0$. In this case the two atoms at the top and bottom of the rhombohedron are perfectly isolated as shown in Fig.4(a). The $1/2$ fractional charge appears at each of the two corners of the rhombohedron as shown in Fig.4(e). These zero-energy states are protected by the chiral symmetry and remain as they are as long as the bulk band gap does not close.

v) We finally analyze the WC. It is easy to derive this at $t_a = 0$, where the eigen function for the valence band is given by $\psi = \left(-e^{i(k_x+k_y+k_z)}, 1\right)/\sqrt{2}$. The WC is calculated as $(1/2, 1/2, 1/2)$ for $|t_a| < t_b/3$. The gap closes at $|t_a| = t_b/3$, and the system becomes semimetallic for $|t_a| > t_b/3$, as shown in 4(d).

Conclusion: We have proposed minimal models for Wannier-type HOTIs. They are given by chiral-symmetric two-band models. We have demonstrated that the WC is identical to the winding number in these models. The construction of a Wannier-type HOTI based on a nontrivial WC will be applicable to other lattices with dimerizations. We have also discussed the physics of phosphorene in the vicinity of the Fermi energy by making a perturbation of a Wannier-type HOTI. We have predicted the emergence of two corner states in a rhombus structure around -0.16eV.

The author is very grateful to N. Nagaosa for helpful discussions on the subject. This work is supported by the Grants-in-Aid for Scientific Research from MEXT KAKENHI (Grants No. JP15H05854, No. JP17K05490 and No. JP18H03676). This work is also supported by CREST, JST (JPMJCR16F1).

[1] M. Z. Hasan and C. L. Kane, Rev. Mod. Phys. **82**, 3045 (2010).
[2] X.-L. Qi and S.-C. Zhang, Rev. Mod. Phys. **83**, 1057 (2011).
[3] F. Zhang, C.L. Kane and E.J. Mele, Phys. Rev. Lett. **110**, 046404 (2013).
[4] W. A. Benalcazar, B. A. Bernevig, and T. L. Hughes, 10.1126/science.aah6442.
[5] F. Schindler, A. Cook, M. G. Vergniory, and T. Neupert, in APS March Meeting (2017).
[6] Y. Peng, Y. Bao, and F. von Oppen, Phys. Rev. B **95**, 235143 (2017).
[7] J. Langbehn, Y. Peng, L. Trifunovic, F. von Oppen, and P. W. Brouwer, Phys. Rev. Lett. **119**, 246401 (2017).
[8] Z. Song, Z. Fang, and C. Fang, Phys. Rev. Lett. **119**, 246402 (2017).
[9] W. A. Benalcazar, B. A. Bernevig, and T. L. Hughes, Phys. Rev. B **96**, 245115 (2017).
[10] F. Schindler, A. M. Cook, M. G. Vergniory, Z. Wang, S. S. P. Parkin, B. A. Bernevig, and T. Neupert, Science Advances 4, eaat0346 (2018).
[11] M. Lin and T. L. Hughes, arXiv:1708.08457.
[12] M. Ezawa, Phys. Rev. Lett. 120, 026801 (2018).
[13] H. C. Po, A. Vishwanath, and H. Watanabe, Nature Communications 8, 50 (2017).
[14] B. Bradlyn, L. Elcoro, J. Cano, M. G. Vergniory, Z. Wang, C. Felser, M. I. Aroyo, and B. A. Bernevig, Nature 547, 298 (2017).
[15] M. Ezawa, Phys. Rev. B, **73**, 045432 (2006).
[16] M. Ezawa, Phys. Rev. B **76**, 245415 (2007).
[17] W. P. Su, J. R. Schrieffer, and A. J. Heeger, Phys. Rev. Lett. **42**, 1698 (1979).
[18] B. Wunsch, F. Guinea and F. Sols, New J. of Phys., 10, 103027 (2008).
[19] G. Montambaux, F. Piechon, J.-N. Fuchs, and M. O. Goerbig,

Phys. Rev. B 80, 153412 (2009).
[20] V.M. Pereira,A.H. Castro Neto and N.M.R. Peres, Phys. Rev. B **80**, 045401 (2009).
[21] G. Montambaux, F. Piéchon, J.-N. Fuchs, and M. O. Goerbig, Phys. Rev. B **80**, 153412 (2009).
[22] M. Ezawa, New J. Phys. **16**, 115004 (2014).
[23] R. Takahashi and S. Murakami, Phys. Rev. B 88, 235303 (2013).
[24] A. N. Rudenko and M.I. Katsnelson, Phys. Rev. B **89**, 201408 (2014).
[25] M. M. Grujic, M. Ezawa, M. Z. Tadic, F. M. Peeters, Phys. Rev. B **93**, 245413 (2016).